3D Superstructures

DOI: 10.1002/ange.201408247

Growth and Origami Folding of DNA on Nanoparticles for High-Efficiency Molecular Transport in Cellular Imaging and Drug Delivery**

Juan Yan, Chongya Hu, Ping Wang, Bin Zhao, Xiangyuan Ouyang, Juan Zhou, Rui Liu, Dannong He, Chunhai Fan, and Shiping Song**

Abstract: *A novel three-dimensional (3D) superstructure based on the growth and origami folding of DNA on gold nanoparticles (AuNPs) was developed. The 3D superstructure contains a nanoparticle core and dozens of two-dimensional DNA belts folded from long single-stranded DNAs grown in situ on the nanoparticle by rolling circle amplification (RCA). We designed two mechanisms to achieve the loading of molecules onto the 3D superstructures. In one mechanism, ligands bound to target molecules are merged into the growing DNA during the RCA process (merging mechanism). In the other mechanism, target molecules are intercalated into the double-stranded DNAs produced by origami folding (intercalating mechanism). We demonstrated that the as-fabricated 3D superstructures have a high molecule-loading capacity and that they enable the high-efficiency transport of signal reporters and drugs for cellular imaging and drug delivery, respectively.*

Inorganic nanoparticles have attracted considerable attention as nanocarriers for cellular imaging and drug delivery owing to their unique properties, such as their high surface-to-volume ratio, optical behavior, and the ability to be functionalized with biomolecules.[1–4] However, many studies have shown that the practical use of nanoparticles as nanocarriers is often hampered either by the low molecule-loading capacity of small nanoparticles owing to their limited surface areas or by the low-efficiency cellular uptake and low intracellular stability of large nanoparticles.[5–10] More recently, DNA nanostructures based on self-assembled DNA nanotechnology have shown great promise as nanocarriers.[11–19] For example, the use of three-dimensional (3D) DNA nanostructures for the controlled release of nanocargo has been reported.[12,20,21] However, current 3D DNA nanostructures still suffer from complicated structure designs, a low yield, the high cost of hundreds of staple strands, and time-consuming annealing procedures.[22]

Herein, we designed a strategy to fabricate a novel 3D gold–DNA superstructure based on the growth and origami folding of DNA on gold nanoparticles (AuNPs; Scheme 1); this strategy combines the rigidity of nanoparticles with the flexibility of DNA nanostructures.

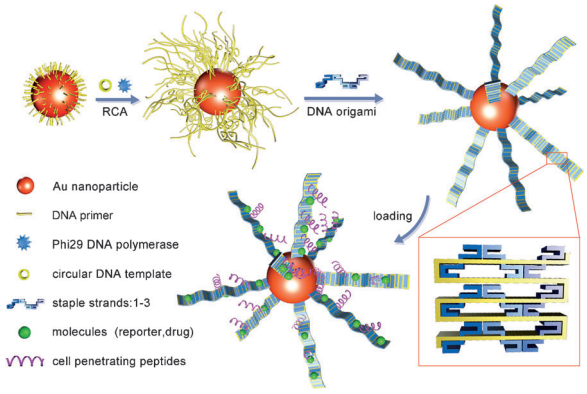

Scheme 1. Illustration of the fabrication of Au-DNA 3D superstructures based on DNA growth and origami techniques at the nano–bio interface. The growth of DNA is initiated by RCA, producing dozens of long ssDNA strands on single AuNPs. The folding of the long ssDNA is accomplished by an origami technique, producing DNA belts on the AuNPs.

Each 3D superstructure contains a 10 nm nanoparticle core and dozens of two-dimensional (2D) DNA belts folded from long single-stranded DNAs (ssDNAs) that are grown in situ on the nanoparticle by rolling circle amplification (RCA). The origami folding of the DNA belts is simple and requires only three staple strands. Each DNA belt is approximately 16 nm in width and several hundred nanometers in length. We demonstrated that the as-fabricated 3D superstructures have a high molecule-loading capacity. More importantly, the superstructures enabled the high-efficiency transport of signal reporters and drugs for cellular imaging and drug delivery, respectively.

In the typical 3D superstructures fabrication process (Scheme 1), oligonucleotides that serve as DNA primers are

[*] Dr. J. Yan, Dr. P. Wang, J. Zhou, R. Liu, Prof. D. He
National Engineering Research Center for Nanotechnology
Shanghai 200241 (China)
Dr. J. Yan, Dr. B. Zhao, Dr. X. Ouyang, Prof. C. Fan, Prof. S. Song
Laboratory of Physical Biology
Shanghai Institute of Applied Physics
Chinese Academy of Sciences, Shanghai 201800 (China)
E-mail: spsong@sinap.ac.cn
C. Hu, Prof. D. He
School of Materials Science and Engineering
Shanghai JiaoTong University, Shanghai 200240 (China)
E-mail: hdn_nercn@163.com

[**] We thank the National Basic Research Program of China (973 program, 2013CB932800 and 2012CB932600), the National Science Foundation of China (91127037, 91123037, 21373260, 21373260, and 21305088), and Shanghai Science and Technology Development Funds (13QB1402100) for financial support.

Supporting information for this article is available on the WWW under http://dx.doi.org/10.1002/anie.201408247.

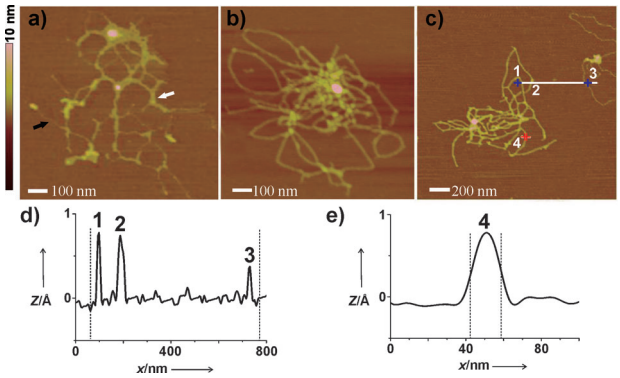

Figure 1. a) AFM image of unfolded RCA products on AuNPs. White arrow: aggregated ssDNAs; black arrow: stretched ssDNAs. b) AFM image of folded RCA products on AuNPs (3D superstructures). c) Comparison of the unfolded and folded Au-DNA nanostructures using AFM imaging. The four marked positions indicate the heights of the folded ssDNA (positions 1 and 2 in d) and the unfolded ssDNA (position 3 in d) and the width of the folded ssDNA (position 4 in e), illustrating changes in the DNA structures. See Figure S2 c,e in the Supporting Information for AFM images at lower magnification.

assembled on 10 nm AuNPs. RCA,[23–25] an isothermal nucleic acid amplification strategy, is then used to grow the DNA in situ. The DNA primers on the AuNPs initiate RCA in the presence of a circular DNA template, nucleotides, and a phi29 polymerase, thereby generating long ssDNAs.[26] Each long ssDNA comprises hundreds of DNA copies that can hybridize with the circular DNA template. Atomic force microscopy (AFM) imaging revealed that the micrometer-long DNA strands were outstretched from the AuNPs (Figure 1 a). Note that most of the long ssDNAs tend to intertwine rather than stretch and to aggregate around the AuNPs owing to the exposure of the basic groups, the flexibility of the sugar-phosphate backbones, and the electrostatic attraction between the polyanionic backbones and the positively charged AuNPs.[27] Next, DNA origami is used to rearrange the long ssDNAs. Three staple strands of DNA are designed to hybridize with the long ssDNAs and to fold them onto the surfaces of the AuNPs into specific DNA nanostructures with uniform sizes. Different amounts of staple strands of DNA are used alternately to choose the most suitable amount (Supporting Information, Figure S1). Furthermore, AFM images (Supporting Information, Figure S2a–e) were used to examine the structural changes of DNA on the surface of AuNPs in RCA and during the origami process (control groups: Supporting Information, Figure S2h–i).

AFM images revealed that the long ssDNAs became uniform and exhibited a certain width and rigidity after the DNA origami folding (Figure 1 b). Software analysis of the AFM images revealed the changes in the size of the DNA before and after origami folding (Figure 1 c,d). The three positions marked in Figure 1 c (1, 2, and 3) were measured to show the height of the DNA before and after origami folding (Figure 1 d). Position 3, located on the long ssDNA grown by RCA, has a height of approximately 0.5 nm, consistent with the diameter of ssDNA reported in previous studies.[28,29] Positions 1 and 2, located on the folded DNA, have heights of approximately 1 nm, consistent with the diameter of double-stranded DNA (dsDNA), as reported in previous studies.[22] An average width of approximately 16 nm was measured at position 4 (Figure 1 e), demonstrating that the folded DNAs are long and thin belts. Control experiments confirm that both the height and width of dsDNAs are significantly less than those of the DNA-belts (Supporting Information, Figure S3).

Dynamic light scattering experiments were then conducted to measure changes in the hydrodynamic radii of the following different Au-DNA nanostructures: AuNP-DNA primer (Au-primer), RCA-based AuNP-ssDNAs (Au-RCAs), and AuNP-DNA belts (Au-belts) (Supporting Information, Figure S4). The hydrodynamic radii of the Au-RCAs and the Au-belts were approximately 84 nm and 573 nm, respectively, indicating that the long ssDNAs were wrapped around the AuNPs, whereas the DNA belts that were folded from the ssDNAs stretched away from the AuNPs. The results also demonstrated that the flexible and disordered ssDNAs opened and formed relatively rigid and uniform DNA nanostructures during the DNA origami process, resulting in the much greater average radius of the novel 3D superstructures relative to the Au-RCAs. 3D Au-DNA superstructures with different sizes can be fabricated by controlling the RCA process. For each differently sized 3D Au-DNA superstructure, the length and efficiency of the RCA extension are variable within each AuNP and amongst AuNPs owing to the inherent properties of RCA. Additionally, the origami efficiency is affected by the increasing number of primers on AuNPs. We balanced the number of primers and their growth and folding to achieve improved molecule-loading efficiency.

Two mechanisms are used to load molecules onto the 3D superstructures. In one mechanism, ligands bound to target molecules are merged into the growing DNA during the RCA process (merging mechanism). In the second mechanism, target molecules are intercalated into the dsDNA produced by origami folding (intercalating mechanism).

We first determined the molecule-loading efficiency of the merging mechanism using the avidin-biotin system. During the RCA process, biotin labels can be incorporated into the long RCA-generated ssDNA via the use of biotinylated adenosine-5′-triphosphate (biotin-dATP). The specific binding of biotin to avidin (or avidin conjugates) is used to load biomolecules onto the DNA strands. Before the origami folding, the long ssDNAs mainly intertwine and wrap around the AuNPs, leading to the creation of hidden biotin-binding sites. Consequently, the Au-RCAs exhibited very low molecule-loading capacity (Figure 2 a). However, during the origami process, specific biotin sites become well defined and exposed to avidin. AFM imaging revealed the high efficiency molecule loading onto the 3D superstructures (Figure 2 c). Figure 2 b and Figure 2 d illustrate the heights of the positions marked in Figure 2 a and Figure 2 c, respectively. The measured average heights of approximately 10 nm and 4 nm were consistent with the diameters of the AuNPs and streptavidin, respectively. In addition to the origami-based rearrangement of the active biotin sites in the RCA-produced ssDNAs, more biotin labels were incorporated during the

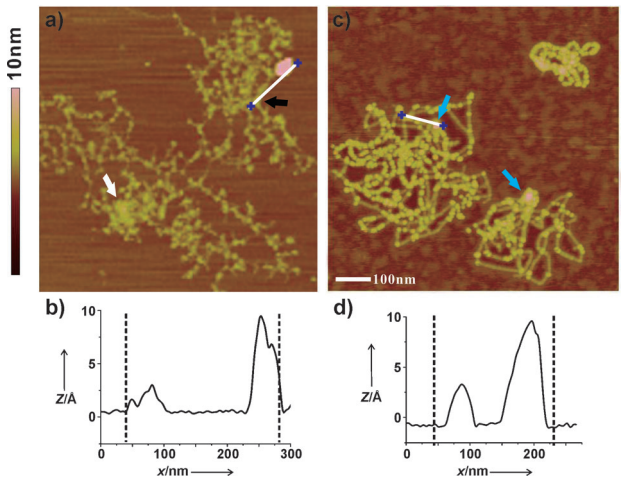

Figure 2. Molecule-loading capacity of the Au-DNA structures by the merging mechanism. a) AFM image of avidin-loaded Au-RCAs. White arrow: aggregated ssDNA. Black arrow: avidin-loaded ssDNA. b) The height of the AuNPs and avidin on the Au-RCAs. c) AFM image of avidin-loaded 3D superstructures (Au-belts). Blue arrow: AuNPs. d) The height of the AuNP and avidin on the 3D superstructures. See Figure S2 f,g in the Supporting Information for AFM images at lower magnification.

DNA origami process by modifying one of the staple strands with biotin. Thus, the 3D superstructures possessed many uniform and exposed biotin sites, allowing the high-efficiency loading of avidin molecules. We demonstrated that the DNA origami folding was extremely efficient despite being conducted on the nanoparticle surfaces. The currently non-optimized origami-folding procedure enabled the high-yield formation of 3D superstructures (Supporting Information, Figure S5).

Having established that the origami-based merging mechanism enables high-efficiency molecule loading, we employed this system to load quantum dots (QDs) onto the 3D superstructures for cellular imaging as a proof of concept for drug delivery. QDs possess excellent optical properties, including a high fluorescent quantum yield, broad absorption/narrow emission, and high photostability; thus, QDs are high-performance fluorescent dyes in cellular imaging.[30–34] However, their applications in cellular imaging suffer from various problems, including poor cellular uptake.[35–37] U87 MG cells, a glioblastoma cell line, were chosen as the target cells. Glioblastoma is reportedly the most aggressive and frequent primary malignant brain tumor in humans.[38,39] QD-linked avidin (QD-Av) and cell-penetrating peptides (CPPs) were co-loaded onto the 3D superstructures through avidin-biotin binding and electrostatic interactions, respectively.[40] The 3D superstructures co-loaded with QDs and CPPs (QD-CPP@3D) were incubated with U87 MG cells for cellular uptake (Figure 3a). After incubation for two hours, the living cells were washed, fixed, and treated with 4,6-diamidino-2-phenylindole dihydrochloride (DAPI) for observation under confocal microscopy. QD-Av and CPP mixtures (QD/CPP) and the QD-loaded 3D superstructures (QD@3D) with equal amounts of QDs were employed as controls. As shown in Figure 3b, very strong red fluorescence was visible inside the

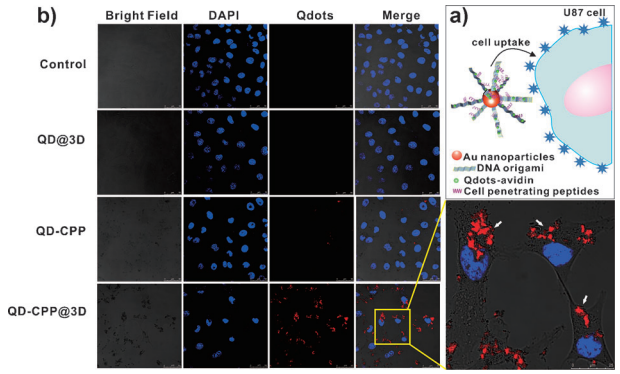

Figure 3. a) Illustration of QD-Av and CPPs co-loaded onto the 3D superstructures (QD-CPP@3D) for cellular uptake. b) Confocal imaging of living U87 cells treated with QD-CPP@3D, QD/CPP, and QD@3D. Inset: magnified image of the QD-CPP@3D-treated U87 cells. The final concentrations of the QDs and CPPs were 2.5 μM and 2 μM, respectively.

U87 MG cells treated with the QD-CPP@3D, demonstrating high-efficiency transport of the QDs on the 3D structures with the aid of the CPPs. However, the QD/CPP-treated cells exhibited very weak fluorescence, whereas the QD@3D-treated cells exhibited no fluorescence; this result indicates not only that CPPs are necessary for QD transport but also that CPPs must coexist with the QDs in the carriers for optimal performance. In this experiment, the origami-based 3D superstructures provided appropriate loading spaces for both the QDs and the CPPs. It was previous demonstrated that the cell uptake of CPP-like large nanostructures might occur through an internalization process based on the energy-independent cell penetration of membranes mediated by CPPs.[41–44]

We then utilized the intercalating mechanism of doxorubicin to characterize the molecule-loading efficiency of the origami-based 3D superstructures. Doxorubicin has been used to treat a wide range of cancers; it intercalates into dsDNA and inhibits macromolecular biosynthesis.[17,45] In our design, after a 24 h incubation period, doxorubicin was intercalated into the DNA belts on the nanoparticles to form doxorubicin-loaded 3D superstructures. The intercalation of doxorubicin into dsDNA caused the formation of a dark red precipitate.[17] Higher amounts of precipitate indicate greater intercalation of doxorubicin. Figure 4a indicates that the origami-based 3D superstructures contained much more doxorubicin than did the Au-RCAs, the Au-primers, and the AuNPs.

The 3D superstructures co-loaded with doxorubicin and CPPs (dox-CPP@3D) were then incubated with U87 MG cells to induce cell death. Doxorubicin and CPPs were co-loaded onto Au-RCAs (dox-CPP@Au-RCAs), Au-primers (dox-CPP@Au-primer), and AuNPs (dox-CPP@Au) with equal amounts of doxorubicin (100 μM); No AuNP-used and no doxorubicin-coloaded samples (dox-CPP@RCAs, dox-CPP @origami and CPP @3D) were prepared as controls. As illustrated in Figure 4b, the cytotoxicity of dox-CPP@3D was much higher than that of the controls. The cell-killing efficiency of dox-CPP@3D was 2.5 times higher than that of pure doxorubicin and 2 times higher than that of the Au-

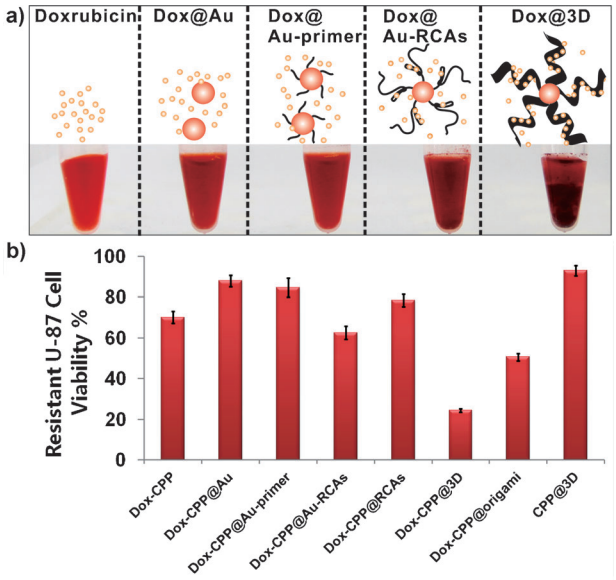

Figure 4. a) Diagram and comparison of nanostructures; b) cell viability of doxorubicin-resistant-U87 cells after incubation with various complexes (100 μM doxorubicin and 2 μM CPPs). CPP@3D (no doxorubicin-loaded group) was used as the control. Error bars represent the standard deviation of three independent experiments performed in triplicate wells containing cells.

RCAs. The results indicate that the origami-based 3D nanostructures not only allow the high-efficiency loading of drugs but also undergo high-efficiency transport, enabling the killing of cancer cells.

In summary, we successfully developed a novel 3D superstructure based on the growth and origami folding of DNA at a nano–bio interface. Combining the rigidity of nanoparticles with the flexibility of DNA nanostructures, the 3D superstructure has several advantages compared with inorganic nanocarriers. First, the molecule-loading capacity of this structure is much higher than that of conventional biomodified inorganic nanocarriers due to the DNA growth and rearrangement. Second, this 3D superstructure has much higher molecular transport efficiency than inorganic nanocarriers because a large number of CPPs can be co-loaded onto the superstructures. Third, the inorganic nanoparticle core and the belted structure can slow the degradation of DNA, allowing the sustained release of drugs in cells. More importantly, the scaffold DNA is obtained using RCA and the staple strands of DNA are very simple, allowing more complex 3D superstructures to be obtained by simply changing the RCA template and staple strands used. Additionally, the rearranged DNAs allow multiple functions to be integrated into a single 3D superstructure. Therefore, the developed strategy can be used to fabricate high-efficiency nanocarriers for the transport of molecules and has great potential regarding applications in molecular assembly, ultrasensitive biodetection, and nanomachines.

Received: August 15, 2014
Revised: October 22, 2014
Published online: January 19, 2015

Keywords: DNA origami · drug delivery · gold nanoparticles · rolling circle amplification

[1] A. Taylor, K. M. Wilson, P. Murray, D. G. Fernig, R. Levy, *Chem. Soc. Rev.* **2012**, *41*, 2707 – 2717.
[2] R. Wilson, *Chem. Soc. Rev.* **2008**, *37*, 2028 – 2045.
[3] L. Dykman, N. Khlebtsov, *Chem. Soc. Rev.* **2012**, *41*, 2256 – 2282.
[4] N. W. Jutaek Nam, J. Bang, H. Jin, J. Park, S. Jung, S. Jung, Y. Park, S. Kim, *Adv. Drug Delivery Rev.* **2013**, *65*, 622 – 648.
[5] Z. Cheng, A. Al Zaki, J. Z. Hui, V. R. Muzykantov, A. Tsourkas, *Science* **2012**, *338*, 903 – 910.
[6] S. Song, Y. Qin, Y. He, Q. Huang, C. Fan, H. Y. Chen, *Chem. Soc. Rev.* **2010**, *39*, 4234 – 4243.
[7] J. M. Nam, C. S. Thaxton, C. A. Mirkin, *Science* **2003**, *301*, 1884 – 1886.
[8] C. A. Mirkin, R. L. Letsinger, R. C. Mucic, J. J. Storhoff, *Nature* **1996**, *382*, 607 – 609.
[9] W. Jiang, B. Y. Kim, J. T. Rutka, W. C. Chan, *Nat. Nanotechnol.* **2008**, *3*, 145 – 150.
[10] T. dos Santos, J. Varela, I. Lynch, A. Salvati, K. A. Dawson, *Small* **2011**, *7*, 3341 – 3349.
[11] R. I. M. N. R. Kallenbach, N. C. Seeman, *Nature* **1983**, *305*, 829 – 831.
[12] E. S. Andersen, M. Dong, M. M. Nielsen, K. Jahn, R. Subramani, W. Mamdouh, M. M. Golas, B. Sander, H. Stark, C. L. Oliveira, J. S. Pedersen, V. Birkedal, F. Besenbacher, K. V. Gothelf, J. Kjems, *Nature* **2009**, *459*, 73 – 76.
[13] P. W. Rothemund, *Nature* **2006**, *440*, 297 – 302.
[14] H. Yan, X. Zhang, Z. Shen, N. C. Seeman, *Nature* **2002**, *415*, 62 – 65.
[15] H. Pei, N. Lu, Y. Wen, S. Song, Y. Liu, H. Yan, C. Fan, *Adv. Mater.* **2010**, *22*, 4754 – 4758.
[16] H. Lee, A. K. Lytton-Jean, Y. Chen, K. T. Love, A. I. Park, E. D. Karagiannis, A. Sehgal, W. Querbes, C. S. Zurenko, M. Jayaraman, C. G. Peng, K. Charisse, A. Borodovsky, M. Manoharan, J. S. Donahoe, J. Truelove, M. Nahrendorf, R. Langer, D. G. Anderson, *Nat. Nanotechnol.* **2012**, *7*, 389 – 393.
[17] Q. Jiang, C. Song, J. Nangreave, X. Liu, L. Lin, D. Qiu, Z. G. Wang, G. Zou, X. Liang, H. Yan, B. Ding, *J. Am. Chem. Soc.* **2012**, *134*, 13396 – 13403.
[18] J. Li, H. Pei, B. Zhu, L. Liang, M. Wei, Y. He, N. Chen, D. Li, Q. Huang, C. Fan, *ACS Nano* **2011**, *5*, 8783 – 8789.
[19] M. Chang, C. S. Yang, D. M. Huang, *ACS Nano* **2011**, *5*, 6156 – 6163.
[20] D. Han, S. Pal, J. Nangreave, Z. Deng, Y. Liu, H. Yan, *Science* **2011**, *332*, 342 – 346.
[21] S. M. Douglas, I. Bachelet, G. M. Church, *Science* **2012**, *335*, 831 – 834.
[22] X. Ouyang, J. Li, H. Liu, B. Zhao, J. Yan, Y. Ma, S. Xiao, S. Song, Q. Huang, J. Chao, C. Fan, *Small* **2013**, *9*, 3082 – 3087.
[23] B. Schweitzer, S. Wiltshire, J. Lambert, S. O'Malley, K. Kukanskis, Z. Zhu, S. F. Kingsmore, P. M. Lizardi, D. C. Ward, *Proc. Natl. Acad. Sci. USA* **2000**, *97*, 10113 – 10119.
[24] F. C. Simmel, *Nanomedicine* **2007**, *2*, 817 – 830.
[25] W. Zhao, M. M. Ali, M. A. Brook, Y. Li, *Angew. Chem. Int. Ed.* **2008**, *47*, 6330 – 6337; *Angew. Chem.* **2008**, *120*, 6428 – 6436.
[26] W. Zhao, Y. Gao, S. A. Kandadai, M. A. Brook, Y. Li, *Angew. Chem. Int. Ed.* **2006**, *45*, 2409 – 2413; *Angew. Chem.* **2006**, *118*, 2469 – 2473.
[27] S. J. Hurst, A. K. Lytton-Jean, C. A. Mirkin, *Anal. Chem.* **2006**, *78*, 8313 – 8318.
[28] Z. Cheglakov, Y. Weizmann, A. B. Braunschweig, O. I. Wilner, I. Willner, *Angew. Chem. Int. Ed.* **2008**, *47*, 126 – 130; *Angew. Chem.* **2008**, *120*, 132 – 136.
[29] S. Beyer, P. Nickels, F. C. Simmel, *Nano Lett.* **2005**, *5*, 719 – 722.

[30] M. Bruchez, Jr., M. Moronne, P. Gin, S. Weiss, A. P. Alivisatos, *Science* **1998**, *281*, 2013 – 2016.
[31] X. Gao, Y. Cui, R. M. Levenson, L. W. Chung, S. Nie, *Nat. Biotechnol.* **2004**, *22*, 969 – 976.
[32] I. L. Medintz, H. T. Uyeda, E. R. Goldman, H. Mattoussi, *Nat. Mater.* **2005**, *4*, 435 – 446.
[33] X. Michalet, F. F. Pinaud, L. A. Bentolila, J. M. Tsay, S. Doose, J. J. Li, G. Sundaresan, A. M. Wu, S. S. Gambhir, S. Weiss, *Science* **2005**, *307*, 538 – 544.
[34] J. Yan, M. Hu, D. Li, Y. He, R. Zhao, X. Y. Jiang, S. P. Song, L. H. Wang, C. H. Fan, *Nano Res.* **2008**, *1*, 490 – 496.
[35] M. Howarth, W. H. Liu, S. Puthenveetil, Y. Zheng, L. F. Marshall, M. M. Schmidt, K. D. Wittrup, M. G. Bawendi, A. Y. Ting, *Nat. Meth.* **2008**, *5*, 397 – 399.
[36] J. M. Klostranec, W. C. Chan, *Adv. Mater.* **2006**, *18*, 1953 – 1964.
[37] Y. Su, M. Hu, C. Fan, Y. He, Q. Li, W. Li, L. H. Wang, P. Shen, Q. Huang, *Biomaterials* **2010**, *31*, 4829 – 4834.
[38] J. Polivka, Jr., J. Polivka, V. Rohan, O. Topolcan, *J. Ferda*, *Anticancer Res.* **2012**, *32*, 2935 – 2946.
[39] Y. Yang, Z. Yan, D. Wei, J. Zhong, L. Liu, L. Zhang, F. Wang, X. Wei, C. Xie, W. Lu, D. He, *Nanotechnology* **2013**, *24*, 405101.
[40] F. Simeoni, M. C. Morris, F. Heitz, G. Divita, *Nucleic Acids Res.* **2003**, *31*, 2717 – 2724.
[41] Y. S. Choi, A. E. David, *Curr. Pharm. Biotechnol.* **2014**, *15*, 192 – 199.
[42] T. Teesalu, K. N. Sugahara, V. R. Kotamraju, E. Ruoslahti, *Proc. Natl. Acad. Sci. USA* **2009**, *106*, 16157 – 16162.
[43] G. Tunnemann, R. M. Martin, S. Haupt, C. Patsch, F. Edenhofer, M. C. Cardoso, *FASEB J.* **2006**, *20*, 1775 – 1784.
[44] S. Trabulo, A. L. Cardoso, M. Mano, M. C. Pedroso de Lima, *Pharmaceuticals* **2010**, *3*, 961 – 993.
[45] W. J. Pigram, W. Fuller, L. D. Hamilton, *Nature New Biol.* **1972**, *235*, 17 – 19.

